Inherent Structure-Based Multiview Learning With Multitemplate Feature Representation for Alzheimer's Disease Diagnosis

Mingxia Liu, Daoqiang Zhang*, Ehsan Adeli, *Member, IEEE*, and Dinggang Shen*, *Senior Member, IEEE*

Abstract—Multitemplate-based brain morphometric pattern analysis using magnetic resonance imaging has been recently proposed for automatic diagnosis of Alzheimer's disease (AD) and its prodromal stage (i.e., mild cognitive impairment or MCI). In such methods, multiview morphological patterns generated from multiple templates are used as feature representation for brain images. However, existing multitemplate-based methods often simply assume that each class is represented by a specific type of data distribution (i.e., a single cluster), while in reality, the underlying data distribution is actually not preknown. In this paper, we propose an inherent structure-based multiview leaning method using multiple templates for AD/MCI classification. Specifically, we first extract multiview feature representations for subjects using multiple selected templates and then cluster subjects within a specific class into several subclasses (i.e., clusters) in each view space. Then, we encode those subclasses with unique codes by considering both their original class information and their own distribution information, followed by a multitask feature selection model. Finally, we learn an ensemble of view-specific support vector machine classifiers based on their, respectively, selected features in each view and fuse their results to draw the final decision. Experimental results on the Alzheimer's Disease Neuroimaging Initiative database demonstrate that our method achieves promising results for AD/MCI classification, compared to the state-of-the-art multitemplate-based methods.

Index Terms—Multitask feature selection, multitemplate, multiview representation, Alzheimer's disease (AD), disease diagnosis.

M. Liu is with the Department of Radiology and Biomedical Research Imaging Center, University of North Carolina at Chapel Hill, Chapel Hill, NC 27599, USA, and also with the School of Computer Science and Technology, Nanjing University of Aeronautics & Astronautics, Nanjing 210016, China.
*D. Zhang is with the School of Computer Science and Technology, Nanjing University of Aeronautics and Astronautics, Nanjing 210016, China (e-mail: dqzhang@nuaa.edu.cn).
E. Adeli is with the Department of Radiology and Biomedical Research Imaging Center, University of North Carolina at Chapel Hill, Chapel Hill, NC 27599, USA.
*D. Shen is with the Department of Radiology and Biomedical Research Imaging Center, University of North Carolina at Chapel Hill, Chapel Hill, NC 27599, USA, and also with the Department of Brain and Cognitive Engineering, Korea University, Seoul 02841, Korea (e-mail: dgshen@med.unc.edu).
Color versions of one or more of the figures in this paper are available online at http://ieeexplore.ieee.org.

I. INTRODUCTION

ALZHEIMER'S disease (AD), characterized by progressive impairment of cognitive and memory function, is the sixth leading cause of death in the United States for Americans aged 65 years or older. According to a recent report from Alzheimer's Association [1], the total estimated prevalence of AD is expected to be 13.8 million in the United States by 2050. As there is no cure for AD to reverse its progression, it is of vital importance for early diagnosis and monitoring of AD at its early prodromal stage, i.e., mild cognitive impairment (MCI).

In the literature, many brain morphometric pattern analysis methods have been developed for computer-aided AD/MCI diagnosis, by identifying differences in shape and neuroanatomical configuration of different brains provided by magnetic resonance imaging (MRI) [2]–[10]. Most of early works use regional measurement of anatomical volumes in predefined regions of interest (ROIs) (e.g., hippocampus, entorhinal cortex, and neocortex) to investigate abnormal tissue structure caused by AD or MCI. However, it is difficult to accurately label those ROIs, since the prior knowledge about abnormal regions is not always available in practice. More recently, with the development of deformable image registration techniques, automatic spatial normalization proves to be a fundamental procedure in brain morphometric pattern analysis, which allows quantitative comparisons among different subjects in a common space. Within the spatial normalization framework, a large number of brain morphometric analysis methods are developed for automatic AD/MCI diagnosis, e.g., deformation-based morphometry (DBM) [4], [11]–[14], tensor-based morphometry (TBM) [6], [15]–[20], and voxel-based morphometry (VBM) [21]–[26]. Particularly, DBM uses deformation fields to identify relative shape differences between groups of individual brains; TBM measures the Jacobian of deformation fields to localize differences of brain structures, whereas VBM compares brain images on a voxel basis, after deformable registration of individual brain images. For instance, Teipel *et al.* [13] develop a multivariate DBM method to predict AD in MCI, while Lau *et al.* [27] propose to use DBM method to determine longitudinal neuroanatomical changes in AD. Hua *et al.* [20] develop several TBM methods to characterize brain atrophy in AD and MCI, which shows high statistical power to track brain changes in large neuroimaging studies. Shen and Davatzikos [28] propose a high-resolution VBM method by using a mass-preserving deformation mechanism and an automatic spatial normalization approach, achieving a high accuracy of registration. Fan *et al.* [29] design a COMPARE (Classification Of Morphological

Patterns using Adaptive Regional Elements) algorithm to extract volumetric features from spatially adaptive local regions, which overcomes the limitation of traditional voxel-based methods often with very high feature dimensionality and noisy features and has been successfully applied to several MRI-based applications (e.g., AD classification and gender classification [29], [30]).

In general, existing brain morphometric studies usually focus on using only one template as the benchmark space to compare anatomic differences among different brains. Actually, using only a single template may cause a bias in registration, as the template may have shape and intensity distributions that are closer to some subjects, but not close-enough to other subjects. For instance, it is reported that the statistical power of TBM using only a single template depends on the particular template selected [18], [20]. To address this issue, several multitemplate-based brain morphometric methods have been recently proposed [17], [19], [31]–[33], where all studied MR images are nonlinearly registered onto multiple predefined templates. Compared with single-template-based methods, multitemplate-based methods could achieve overall lower registration error, which leads to less noisy feature representation for subjects [33]. Also, with each template as a specific view, multiview feature representation generated from different templates for a brain image can better represent each subject and could promote the performance of the subsequent learning models. For instance, Leporé et al. [17] develop a multitemplate-based approach for AD classification and achieve better results than single-template-based methods. Koikkalainen et al. [19] and Min et al. [31], [34] propose to extract multiview features from multiple templates for all studied subjects, where features are averaged and concatenated for AD/MCI classification, respectively. To better use multiview features, Liu et al. [32] develop a view-centralized multitemplate classification method by focusing on features from a specific view (i.e., template) with the guidance information from features of other views and achieve promising results for AD/MCI classification.

However, most of existing multitemplate-based methods simply assume that each class is represented by a specific type of data distribution (e.g., Gaussian distribution) [17], [19], [31], [32]. Although such assumption may simplify the problem at hand, it will definitely degrade the learning performance, because the underlying distribution structure of data is actually not preknown. In practice, the potentially complicated distribution structure of neuroimaging data within a specific class could result from several facts [35], e.g., 1) different subtypes of a specific disease, and 2) inaccurate clinical diagnosis. Intuitively, modeling the inherent distribution structure information of data can bring more prior information to the learning process and, thus, could further promote the diagnosis performance. To the best of our knowledge, no previous multitemplate-based methods employ such distribution structure information of data in their learning models.

In this paper, we propose an inherent structure-based multiview learning (ISML) method for AD/MCI classification. Specifically, we first nonlinearly register each brain MR image onto multiple selected templates, through which multiview feature representation for each subject can be obtained from different templates. To uncover the inherent distribution structure of

data, we partition subjects in each original class into several subclasses (i.e., clusters) by using a clustering algorithm. Then, we relabel each subclass with a unique code vector by considering both its original class label and its distribution information. Afterwards, we adopt a multitask feature selection method to select informative features in each view space. Based on those selected features, we then learn multiple support vector machine (SVM) classifiers, with each SVM corresponding to a specific view space. Finally, we fuse these SVMs by an ensemble classification method with a simple majority voting strategy. Experiments on the ADNI database demonstrate that our method outperforms the *state-of-the-art* multitemplate-based methods for AD/MCI classification. The major contributions of this paper are twofold. First, we propose to mine the underlying distribution structure information of data for multitemplate-based methods, by using a subclass clustering algorithm. Second, we develop an ensemble classification method to better take advantage of multiview feature representation generated from multiple templates.

It is worth indicating the difference between this work and our previous study [32]. First, the method proposed in [32] focuses on using the representation from the main view (i.e., template) with extra guidance from other views, where the inherent data structure of multiview data is not considered. In contrast, this study focuses on exploiting the data distribution structure information within each view space, where a clustering-based algorithm is adopted to partition the original data into several subclasses. In addition, feature selection in [32] is performed in each individual view space, where the inherent relationships among different views are not considered. Different from [32], feature selection in this study is under a multitask learning framework, where the relationships among different tasks (with each task corresponding to a specific view) can be modeled implicitly.

The rest of the paper is organized as follows. We first present the details of our proposed approach in Section II. Then, we describe the experiments and comparative results in Section III. In Section IV, we investigate the influence of parameters, analyze the diversity of classifiers, and discuss the limitations of our method. Finally, we conclude this paper in Section V.

II. METHOD

Figure 1 shows the flowchart of our proposed ISML method for AD/MCI classification. From Fig. 1, we can observe that there are three main steps in ISML, including 1) multiview feature extraction, 2) subclass clustering-based feature selection, and 3) SVM-based ensemble classification. In what follows, we will elaborate each step in detail.

A. Multiview Feature Extraction

In this study, we develop a multiview feature extraction method using multiple templates, with each template regarded as a specific view representation. In brief, we first develop a study-specific template selection strategy to obtain multiple templates from data and then extract multiview regional feature representation for each subject from multiple template spaces.

1) Template Selection: In multitemplate-based methods, each brain MR image is usually first nonlinearly registered onto
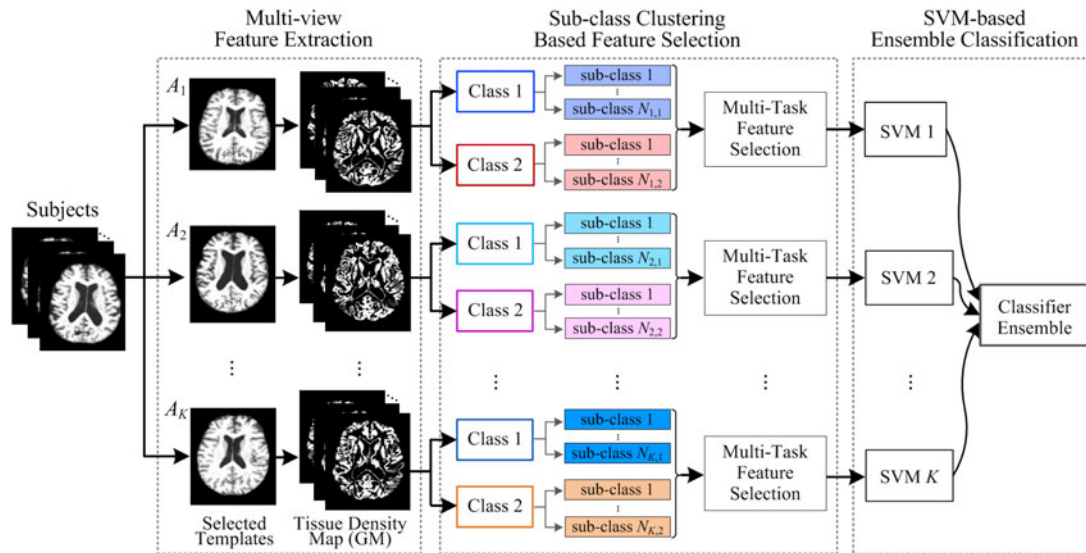
Fig. 1. Flowchart of our proposed method, including three main steps: 1) multiview feature extraction, 2) subclass clustering-based feature selection, and 3) SVM-based ensemble classification.

multiple selected templates, through which multiview feature representation can be extracted by regarding each template as a specific view. In the literature, existing multitemplate-based studies *either* employ templates in a predefined template library [17] *or* select templates randomly from all studied subjects [19]. However, due to differences between populations (e.g., age, disease, etc.) or changes in scanner and imaging technology, MR images in two different studies might be significantly different [19], [35]. Thus, predefined templates and those obtained by random selection strategy may be not representative enough for the whole population in a specific study, which may induce large registration errors and reduce the discriminative ability of the features. Different from previous template selection strategies, we now develop a study-specific template selection approach that can capture population variability as much as possible. In brief, we adopt an affinity propagation (AP) clustering algorithm [36] to partition the studied subjects into several clusters. Thereupon, the corresponding cluster centers (i.e., exemplars) are called and used as templates.

AP starts with a similarity matrix with each element defining the similarity between a pair of data points, and keeps passing real-valued messages between data points until a high-quality set of representative points (i.e., exemplars) and corresponding clusters are found [36]. The advantage of the AP algorithm over traditional clustering algorithms (e.g., k-means [37]) is that AP is independent of the quality of initial sets of cluster centers by considering all data points as cluster centers, simultaneously. In the AP clustering process, we apply a bisection method to find an appropriate preference value [36], while the similarity between two data points is computed as the negative normalized mutual information. In this work, there are a total of ten templates selected from AD and normal controls (NC) subjects (shown in Fig. 2). Although it is possible to select more templates from data, those additional templates could bring more computation burden in the image registration process. On the other hand, the number of our selected templates is similar to existing multitemplate-based studies [17], [19].

2) Feature Extraction: Following [22], we adopt a mass-preserving shape transformation framework to capture the morphometric patterns of all studied subjects using multiple templates, by first performing segmentation and registration to extract volumetric features, then adaptively clustering voxels into ROIs in each specific template space, and finally extracting features from each ROI. Specifically, we first adopt a brain tissue segmentation method [38] to segment each skull-stripped MR brain image into three tissues, i.e., gray matter (GM), while matter (WM), and cerebrospinal fluid (CSF). Since GM is most affected by AD [39], [40], we only use GM tissues for feature extraction and classification in this study. Afterwards, the tissue-segmented brain image (i.e., GM) is spatially normalized onto each of multiple template spaces, by using a high-dimensional image warping method called HAMMER [41]. Given K templates, a total of K GM tissue density maps, each reflecting the local volumetric measurement, are generated from multitemplate spaces for each subject.

The above mass-preserving transformation procedure generates millions of volumetric features for each brain that could be redundant and noisy for subsequent learning model, especially for only a relatively small number of training samples [29], [31], [42]. At the same time, traditional methods for obtaining regional features using predefined ROIs are not suitable for multitemplate-based methods, because different templates may provide complementary representation for a brain image from different views. Following [29], we adopt a watershed segmentation algorithm [43] to obtain a regional grouping of volumetric features in each of multiple template spaces, individually. In this way, different templates will yield different ROI partitions, due to the fact that different tissue density maps of the same subject are generated in different template spaces. Furthermore, other than using all voxels in each region for total regional volumetric measurement, we adopt a regional feature aggregation method to aggregate only a subregion in each region to further optimize the discriminative power of the obtained regional features, by using an iterative voxel selection
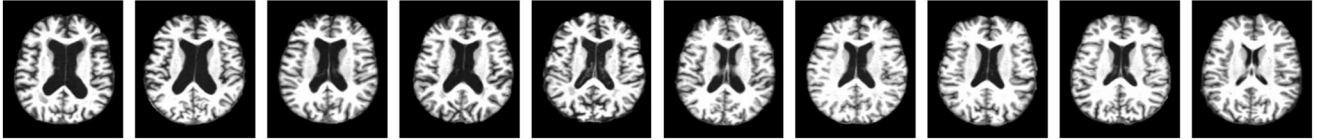
Fig. 2.   Selected templates (i.e., exemplars) achieved by AP algorithm.

algorithm proposed in [29]. Finally, in each template space, D regional features are extracted for each subject. Using K templates, we can obtain K sets of D-dimensional features for each studied subject, while each set of features represents a subject from a specific view (i.e., template). It is worth noting that, compared with the single-view feature extraction method, our multiview feature extraction method has relatively higher computational cost. That is mainly because of using multiple templates for image registration using HAMMER [41]. But this is reasonable, since we are incorporating more information and potentially selecting better and more relevant features. Thus, there is a tradeoff between the quality of feature representation and the computational cost. One possible solution in the future is to parallelize the image registration process by using multiple CPUs, which will speed up multiview feature extraction process.

B. Subclass Clustering-Based Feature Selection

Although we perform voxel selection in the feature extraction stage to improve the discriminative power of features, many regional features could be still redundant or noisy for subsequent classification models because of the limited number of training subjects. Hence, feature selection is an essential step to eliminate those redundant or noisy features. On the other hand, since the data distribution structure of a particular class may be complicated, we believe that mining and utilizing such structure information in the feature selection stage can help find informative features. Accordingly, we first propose to mine the inherent structure of data in each template space, by employing a subclass clustering algorithm. Based on the clustering results, we then encode those subclasses with unique codes by considering both their original class information and their own distribution information, with a popular one-versus-all (OVA) encoding strategy [44]. Afterwards, we utilize a multitask feature selection model to select the most informative features, through which the structure information of data is used to guide the feature selection process.

To uncover the underlying structure of a specific class, we exploit the AP algorithm [36] again to partition the subjects within each class into several subclasses (i.e., clusters) in each of multiview spaces. As an example, Fig. 3 shows the subclass clustering results with subjects belonging to two original classes (i.e., Class 1 and Class 2). Using the AP algorithm, we partition the subjects in Class 1 into two subclasses, and divide subjects in Class 2 into three subclasses (see Fig. 3). Then, we relabel all subclasses with unique codes by encoding the original classes and those subclasses using the OVA encoding strategy, respectively. As illustrated in Fig. 3, each original class is now represented by a unique OVA coding vector (i.e., [1 0] for Class
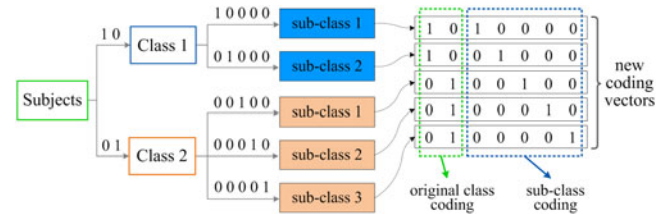

Fig. 3.   Example illustration of our proposed subclass clustering-based encoding method in a specific view space, where subjects in Class 1 are partitioned into two subclasses, while subjects in Class 2 are divided into three subclasses.

1 and [0 1] for Class 2). For those five subclasses in both Class 1 and Class 2, we encode them with similar OVA encoding strategy. Specifically, subclass 1 and subclass 2 in Class 1 are encoded as [1 0 0 0 0] and [0 1 0 0 0], respectively, while those three subclasses in Class 2 are encoded as [0 0 1 0 0], [0 0 0 1 0], and [0 0 0 0 1], respectively. In this way, subjects in subclass 1 of Class 1 are finally labeled as [1 0 1 0 0 0 0], where the first two bits denote the OVA coding for its original class (i.e., Class 1), and the last five bits represent its unique OVA coding among five subclasses of all original classes.

Throughout the paper, we denote matrices as boldface uppercase letters, vectors as boldface lowercase letters, and scalars as normal italic letters. Denote $\mathbf{X} \in \mathbb{R}^{N \times D}$ as the data matrix with N subjects and D-dimensional features in a specific view space. Let $\mathbf{Y} \in \mathbb{R}^{N \times C}$ represent the new class label matrix for N subjects by employing the above subclass clustering-based encoding strategy, where each subject is labeled by a C-bit row vector, and C is the sum of the number of original classes and the number of subclasses of all original classes. Since each column of $\mathbf{Y}$ partitions all studied subjects into two categories in a new label space, the original problem can be transformed into C binary subproblems, where subjects labeled as 1 are treated as positive samples, and those labeled as 0 are used as negative samples. Therefore, we can transform the original problem into a multitask learning problem (e.g., seven tasks in Fig. 3) with each task corresponding to a specific column of $\mathbf{Y}$.

After the subclass clustering and the encoding processes, we then adopt a multitask feature selection model to select informative features in each view space individually. Let $\mathbf{a}_i$ and $\mathbf{a}^j$ represent the ith row and the jth column of a matrix $\mathbf{A}$, respectively. We further denote the Frobenius norm and the $l_{2,1}$ norm of $\mathbf{A}$ as $||\mathbf{A}||_F = \sqrt{\sum_i ||\mathbf{a}_i||_2^2}$ and $||\mathbf{A}||_{2,1} = \sum_i ||\mathbf{a}_i||_2$, respectively. Also, let $\mathbf{W} = [\mathbf{w}^1, \mathbf{w}^2, \ldots, \mathbf{w}^c, \ldots, \mathbf{w}^C] \in \mathbb{R}^{D \times C}$ represent the weight matrix for C learning tasks, and $\mathbf{w}^c$ is a column weight vector corresponding to the cth task. To jointly select common features among different tasks, we adopt

a multitask feature selection model [45], which is defined as

$$\min_{\mathbf{w}} \|\mathbf{Y} - \mathbf{XW}\|_F^2 + \lambda \|\mathbf{W}\|_{2,1} \quad (1)$$

where the first term is the empirical loss on the training data, the second term is a group sparsity regularizer, and λ is a parameter used to trade off the balance between the two terms in (1). Due to the group sparsity nature of $l_{2,1}$ norm [45], the estimated optimal coefficient matrix $\hat{\mathbf{W}}$ will have some zero-value row vectors, implying that the corresponding features are not informative in predicting any of the class labels of the training data. Unlike conventional methods that only learn a single mapping function between the input data and corresponding class labels, our subclass clustering-based multitask learning aims to learn multiple mapping vectors (i.e., $\{\mathbf{w}^1, \mathbf{w}^2, \dots, \mathbf{w}^c, \dots, \mathbf{w}^C\}$) jointly, which allows us to explicitly take advantage of the distribution structure of original classes in the feature selection process. In this study, we used the SLEP toolbox [46] for solving the proposed problem in (1).

C. SVM-Based Ensemble Classification

To better take advantage of multiview feature representation generated from different templates, we further propose an SVM-based ensemble classification approach. Specifically, we first learn a view-specific linear SVM classifier based on the selected features in each view space. Due to the max-margin classification characteristic, the SVM has good generalization capability across different training data (e.g., produced in each tenfold cross-validation case in our experiments), as extensively shown in existing AD diagnosis studies [10], [32], [47]. Given K different views (i.e., templates), we therefore obtain K different SVMs. Note that those SVMs for K views are trained individually, with each one learned by using all studied subjects with feature representation from a specific view space and their original class labels. Then, a majority voting strategy [48], a simple but effective classifier fusion method, is employed to combine the outputs of those view-specific SVMs. Given a new test sample, its class label is determined through the same majority voting of the outputs of K SVM classifiers.

III. EXPERIMENTAL RESULTS

A. Subjects and Image Preprocessing

1) Subjects: In this study, we evaluate the efficiency of our proposed method on the Alzheimer's Disease Neuroimaging Initiative (ADNI) database available at http://adni.loni.usc.edu/. We only consider the T1-weighted MRI baseline data in ADNI-1 database, acquired from 97 AD, 128 NC, and 234 MCI subjects. For those MCI subjects, they were further clinically divided into 117 progressive MCI (pMCI) subjects who progressed to AD in 18 months, and 117 stable MCI (sMCI) subjects who did not progress to AD in 18 months. In Table I, we show the demographic and clinical information of the studied subjects.

In the ADNI database, subjects were 55–90 years old with a study partner who can provide an independent evaluation of functioning. General inclusion/exclusion criteria are briefly listed as follows (see http://www.adni-info.org/Home.aspx). 1) Normal control subjects: Mini-Mental State Examination

TABLE I
DEMOGRAPHIC INFORMATION OF 459 STUDIED SUBJECTS FROM THE ADNI DATABASE

Diagnosis	AD	pMCI	sMCI	NC
Subject number	97	117	117	128
Male/Female	48/49	67/50	79/38	63/65
Age (Mean ± SD)	75.90 ± 6.84	75.18 ± 6.97	75.09 ± 7.65	76.11 ± 5.10
MMSE (Mean ± SD)	23.37 ± 1.84	26.45 ± 1.66	27.42 ± 1.78	29.13 ± 0.96

Note: Values are denoted as mean ± deviation; MMSE means mini-mental state examination; M and F represent male and female, respectively.

(MMSE) scores between 24 and 30 (inclusive), a Clinical Dementia Rating (CDR) of 0, nondepressed, non-MCI, and nondemented; 2) MCI subjects: MMSE scores between 24 and 30 (inclusive), a memory complaint, objective memory loss measured by education adjusted scores on Wechsler Memory Scale Logical Memory II, a CDR of 0.5, absence of significant levels of impairment in other cognitive domains, essentially preserved activities of daily living, and an absence of dementia; and 3) AD subjects: MMSE scores between 20 and 26 (inclusive), CDR of 0.5 or 1.0, and meets the National Institute of Neurological and Communicative Disorders and Stroke and the Alzheimer's Disease and Related Disorders Association (NINCDS/ADRDA) criteria for probable AD.

The MR images for all studied subjects were preprocessed by a standard procedure. Specifically, to correct intensity inhomogeneity, we first perform a nonparametric nonuniform bias correction proposed in [49] for each MR image. Then, skull stripping [3] and manual review or correction are performed to remove both skull and dura, followed by cerebellum removal. Next, each brain image is segmented into three tissues (i.e., GM, WM, and CSF) by using FAST [38]. Finally, all brain images are affine aligned by FLIRT [50], [51].

2) Experimental Setting: The evaluation of our method is conducted on three binary classification problems, including AD versus NC classification, pMCI versus NC classification, and pMCI versus sMCI classification. In the experiments, we use a tenfold cross-validation strategy to evaluate the performance of our method and those compared methods. We randomly partition the studied subjects in each class into ten subsets with approximately equal size without replacement. Afterwards, one subset is used as testing data, while the others are employed as training data. We then report the performances of different methods by averaging the results of those ten folds in cross validation.

We compare the proposed subclass clustering feature selection method with six well-known feature selection methods, including *t*-test [52], Laplacian Score (LS) [53], Fisher Score (FS), Pearson Correlation (PC) [54], COMPARE [29], and LASSO [55]. For LS/FS/PC methods, we first select the top d features from the ranking list of features generated by the corresponding algorithms on the training set, where d is the desired number of selected features specified as $d = \{1, 2, \dots, D\}$ in the experiments. Then, we report the highest classification accuracy achieved by LS/FS/PC on the testing set. For *t*-test, COMPARE, LASSO, and our method, the optimal feature subset is determined through corresponding algorithms on the training

set via inner cross validation, and the classification results on the testing set are reported using such fixed feature subset. In this study, $K = 10$ templates are selected from AD and NC subjects using the AP clustering algorithm, and each subject is represented by a D-dimensional ($D = 1500$ in this study) feature vector in each of templates (i.e., views). For fair comparison, all competing methods share the same multiview feature representation for each training (or testing) subject.

In addition, we deal with multiview features generated from different templates via three different ways. First, we employ single-view features in the first group of experiments. That is, we first perform feature selection in a specific view space (i.e., only features from this view are used) and construct a view-specific SVM classifier using those selected features. We then average the results among multiple single views achieved by different methods. Second, we simply concatenate multiview features generated from multiple templates as a long feature vector and then use different feature selection algorithms to perform feature selection, followed by an SVM classifier. Finally, we make use of multiview features through the proposed SVM-based ensemble classification strategy, where we perform feature selection in each of multiview spaces individually, and construct multiple SVMs (each SVM corresponding to a specific view). This would be followed by a majority voting strategy to combine the outputs of those SVMs for making a final decision.

Following [56], the subclass number of positive classes, i.e., 1) AD in AD versus NC classification, 2) pMCI in pMCI versus NC classification, and (3) pMCI in pMCI versus sMCI classification, in our method is empirically set as 2, while that for negative classes is set as 3. In Section IV, we further investigate the influence of subclass numbers on the learning performance of our method. For model selection, the regularization parameter (i.e., λ) in our subclass clustering-based feature selection model as defined in (1), as well as the parameter for l_1-norm regularizer in LASSO, are both chosen from the range $\{2^{-10}, 2^{-9}, \dots, 2^0\}$ through inner tenfold cross validation on the training data. Specifically, the training data are further divided into ten subsets, with one subset for testing and the other nine subsets for training. Finally, we select the parameter values with which the learning method can achieve the best average validation classification accuracy among ten folds. For the t-test method, the p-value is chosen from $\{0.05, 0.08, 0.10, 0.12, 0.15\}$ via inner cross validation on training data. Also, the soft margin parameter of linear SVM is chosen from the range $\{2^{-10}, 2^{-9}, \dots, 2^5\}$. Here, we resort to the LIBSVM toolbox [57] for SVM classifier learning and the SLEP toolbox [46] for multitask feature learning.

We evaluate the performance of different methods via seven evaluation metrics: classification accuracy (ACC), sensitivity (SEN), specificity (SPE), balanced accuracy (BAC), positive predictive value (PPV), negative predictive value (NPV) [58], and the area under the receiver operating characteristic (ROC) curve (AUC). Denote TP, TN, FP and FN as True Positive, True Negative, False Positive, and False Negative, respectively. Those evaluation metrics are defined as: 1) ACC = (TP+TN)/(TP+TN+FP+FN); 2) SEN = TP/(TP+FN); 3) SPE = TN/(TN+FP); 4) BAC = (SEN+SPE)/2; 5) PPV =
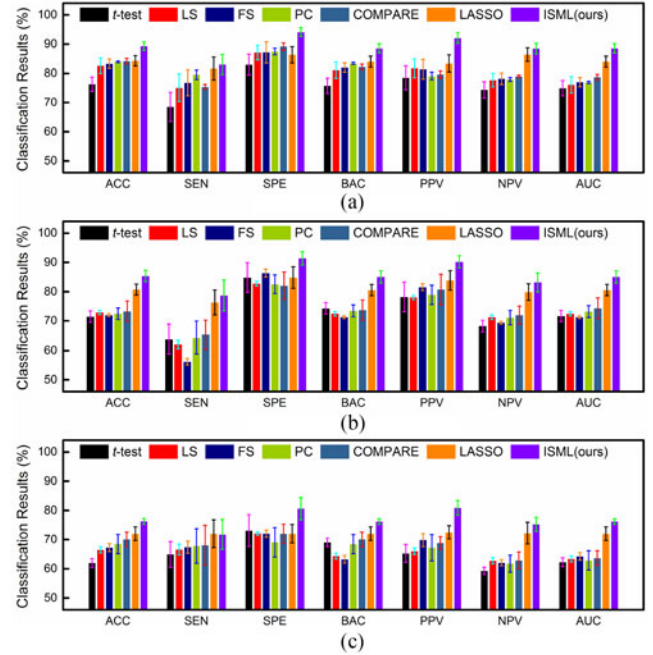

Fig. 4. Averaged classification results achieved by different methods using different single-view features in (a) AD versus NC, (b) pMCI versus NC, and (c) pMCI versus sMCI classification tasks.

TP/(TP+FP); 6) NPV = TN/(TN+FN). In addition, the ROC curve, a plot of true positive rate versus false positive rate, is also used to evaluate the performance of brain disease diagnosis, while the AUC that is a metric for measuring the overall performance of a diagnostic test.

3) Results Using Single-View Features: To demonstrate the superiority of our proposed subclass clustering-based feature selection method, we first perform experiments by using single-view feature representation. Specifically, we first select features in a specific view space using a feature selection algorithm and then construct an SVM classifier with those selected features. Given K sets of single-view features, we report the averaged classification results among K views achieved by different methods in three classification tasks in Fig. 4.

From Fig. 4, one can observe that, in most cases, our method achieves better performance than the compared methods in terms of seven evaluation metrics in three classification problems. Specifically, our ISML method consistently outperforms the compared methods in both the AD versus NC and the pMCI versus NC classification. In pMCI versus sMCI classification, our method is superior to the compared methods in six out of seven evaluation metrics. This indicates that, compared with methods performing direct feature selection according to the original labels, our subclass clustering-based feature selection method helps promote the performance of AD classification. The advantage of our method could be due to the fact that our method utilizes the structure information of data.

4) Results Using Multiview Features via Feature Concatenation: In the second group of experiments, we employ multiview features and feature concatenation strategy to perform classification. That is, we first concatenate multiview features
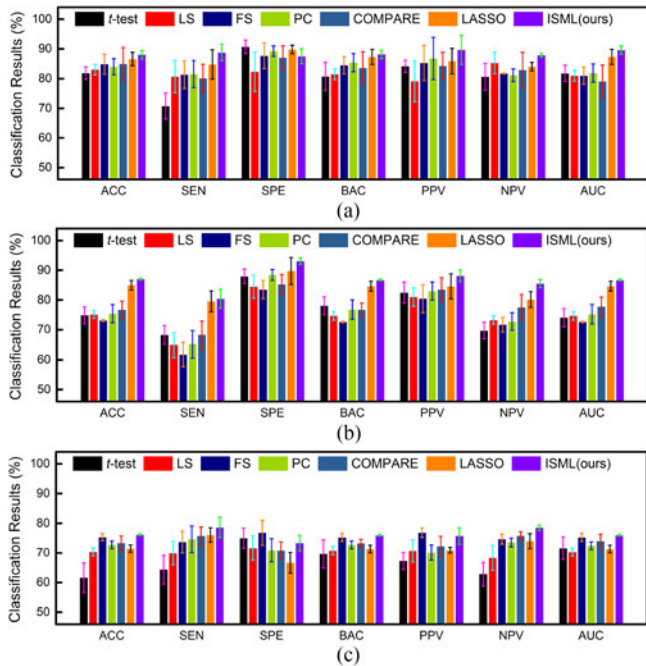
Fig. 5. Classification results achieved by different methods using multiview features and feature concatenation strategy in (a) AD versus NC, (b) pMCI versus NC, and (c) pMCI versus sMCI classification tasks.
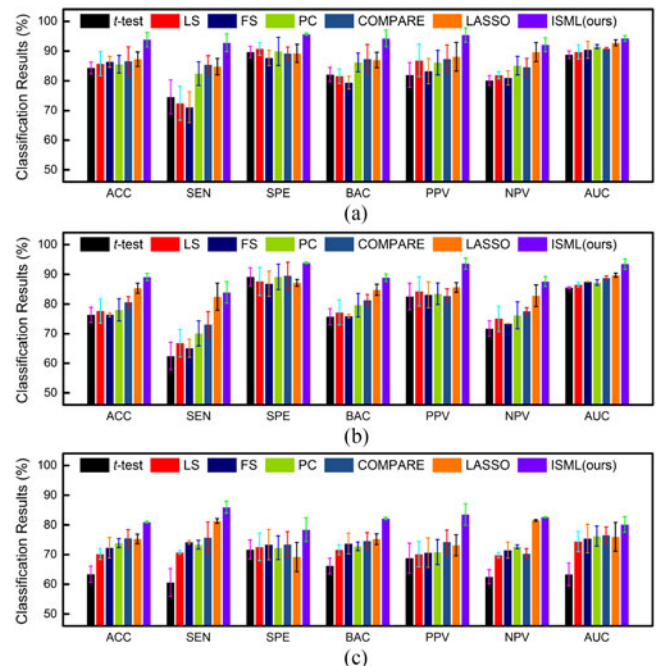

Fig. 6. Classification results achieved by different methods using multiview features and ensemble classification strategy in (a) AD versus NC, (b) pMCI versus NC, and (c) pMCI versus sMCI classification tasks.
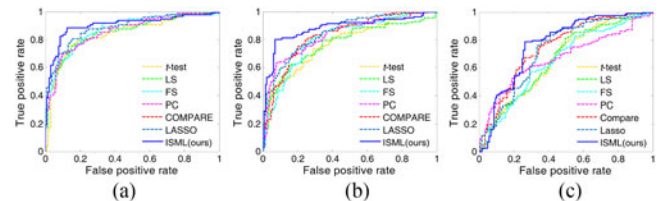

Fig. 7. ROC curves achieved by different methods using the proposed ensemble classification strategy in (a) AD versus NC, (b) pMCI versus NC, and (c) pMCI versus sMCI classification tasks.

generated from different templates as a long feature vector for each subject and then perform feature selection using different algorithms, followed by an SVM classifier. Fig. 5 shows the classification results of different methods using multiview features and the feature concatenation strategy.

As could be seen in Fig. 5, the proposed ISML method outperforms the competing methods, in most cases. For instance, in terms of the classification accuracy, ISML achieves an improvement of 1.44% compared with the second best method (LASSO) in AD versus NC classification, an improvement of 2.03% compared with the second best method (LASSO) in pMCI versus NC classification, and an improvement of 2.78% compared with the second best method (COMPARE) in pMCI versus sMCI classification. On the other hand, from Figs. 4 and 5, one can see that methods using multiview features usually outperform their counterparts using single-view features. This implies that, compared with single-view features, multiview feature representation can facilitate subsequent classification tasks by comprehensively representing each subject.

5) Results Using Multiview Features via Ensemble Classification: In the third group of experiments, we make use of multiview features via our proposed SVM-based ensemble classification strategy. Briefly, we first perform feature selection using a specific feature selection algorithm in each of multiview (i.e., multitemplate) spaces and then construct multiple view-specific SVMs (with each one corresponding to a specific view), followed by a majority voting strategy to combine the outputs of those SVMs for making a final decision. We report the experimental results achieved by different methods in three classification tasks in Fig. 6 and further plot the corresponding ROC curves in Fig. 7.

As shown in both Figs. 6 and 7, our ISML method achieves significantly better performance than other methods in three classification tasks, especially in terms of ACC, SEN, SPE, BAC, PPV, and AUC. In particular, ISML obtains the best sensitivity in AD versus NC classification (7.34% higher than the second best sensitivity achieved by LASSO), indicating that our method can effectively identifies AD (or pMCI) patients. Higher sensitivity values indicate high confidence in disease diagnosis, which is potentially very useful in real-world applications. Thus, from a clinical point of view, ISML is less likely to misdiagnose subjects with diseases, in comparison to those compared methods. In terms of AUC (as shown in Figs. 6 and 7), ISML is apparently superior to all other methods in three classification tasks. In addition, it can be seen from Figs. 5 and 6 that methods using our ensemble classification method generally achieve more promising results, compared with their counterparts using feature concatenation strategy. It implies that the ensemble-based method provides a better way to make use of multiview feature representation, compared with the feature concatenation strategy. Better performance of our ensemble-based method is mainly due to the fact that the rich anatomical

TABLE II
COMPARISON WITH STATE-OF-THE-ART METHODS USING MULTIPLE TEMPLATES IN AD VERSUS NC AND pMCI VERSUS sMCI CLASSIFICATION

Method	Feature Type	Classifier	AD versus NC			pMCI versus sMCI		
			ACC (%)	SEN (%)	SPE (%)	ACC (%)	SEN (%)	SPE (%)
Koikkalainen *et al.* [19]	TBM	Linear regression	86.00	81.00	91.00	72.10	77.00	71.00
Wolz *et al.* [8]	TBM	Linear discriminant analysis	87.00	84.00	90.00	64.00	65.00	62.00
Min *et al.* [31]	Data-Driven ROI GM	SVM	91.64	88.56	93.85	72.41	72.12	72.58
Min *et al.* [34]	Data-Driven ROI GM	SVM	90.69	87.56	93.01	73.69	76.44	70.76
Liu *et al.* [32]	Data-Driven ROI GM	SVM ensemble	92.51	**92.89**	88.33	78.88	85.45	76.06
ISML (ours)	Data-Driven ROI GM	SVM ensemble	**93.83**	92.78	**95.69**	**80.90**	**85.95**	**78.41**

structures of multitemplates that are treated as specific views individually, while such structure information could be lost in the feature concatenation method.

6) Comparison With State-of-the-Art Methods: Furthermore, we compare the results achieved by our ISML method (using multiview features and ensemble classification strategy) with those of the state-of-the-art methods that use MRI data of ADNI subjects. Since very limited studies report the pMCI versus NC classification results, we only report the results of AD versus NC classification and pMCI versus sMCI classification in Table II, respectively. Also, we further list the details of each method in Table II, including the type of features and classifiers. It is worth noting that 30 templates are randomly selected from all studied subjects in [8] and [19], while ten templates are determined by the AP clustering algorithm from AD and NC subjects in [31], [32], and [34] and our method.

It can be seen from Table II that our ISML method generally outperforms the compared methods in AD versus NC classification. More specifically, ISML achieves much higher accuracy (i.e., 93.83%) and much better specificity (i.e., 95.69%) compared with the other methods and obtains a comparable sensitivity (i.e., 92.78%) compared with the second best method proposed by Liu *et al.* [32]. From Table II, one can also observe that, in pMCI versus sMCI classification, ISML achieves an accuracy of 80.90%, a sensitivity of 85.95%, and a specificity of 78.41%, while the best accuracy, the best sensitivity, and the best specificity obtained by the compared methods are only 78.88%, 85.45%, and 76.06%, respectively. Note that our method is the first one to mine and utilize the underlying complex data distribution structure for feature selection in multitemplate-based methods, while conventional methods simply assume that data are represented by a specific type of distribution (e.g., Gaussian distribution) [8], [19], [31], [32], [34].

IV. DISCUSSION

Since there are two key stages (i.e., subclass clustering-based feature selection and SVM-based ensemble classification) in our ISML method, we further investigate the influence of subclass number on the learning performance and analyze the diversity of classifiers in the classifier ensemble.

A. Influence of Subclass Number

First, we evaluate the influence of different subclass numbers on the learning performance of our ISML method in three
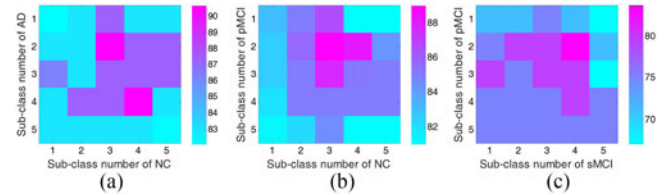

Fig. 8. Classification accuracy versus subclass number, achieved by our ISML method using *feature concatenation strategy* in (a) AD versus NC, (b) pMCI versus NC, and (c) pMCI versus sMCI classification tasks.
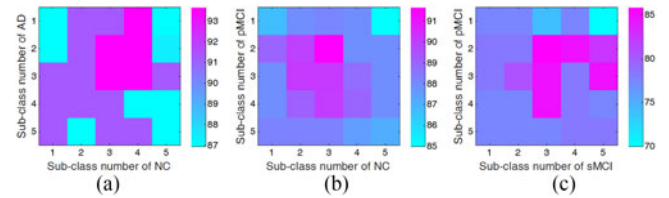

Fig. 9. Classification accuracy versus subclass number, achieved by our ISML method using *ensemble classification strategy* in (a) AD versus NC, (b) pMCI versus NC, and (c) pMCI versus sMCI classification tasks.

classification tasks using multiview feature representation. Following [56], the subclass number for a specific original class (e.g., AD, NC, pMCI, or sMCI) varies from 1 to 5 in our experiments, and the corresponding AP clustering algorithm is performed to partition the subjects within each class into a specific number of clusters. In Figs. 8 and 9, we plot the classification accuracies achieved by ISML with different subclass numbers, using the feature concatenation and the ensemble classification strategies, respectively.

From Figs. 8(a) and 9(a), we can draw the conclusion that ISML achieves the best performance when the subclass number is 2 or 3 for AD, and 3 or 4 for NC. When the subclass number is smaller than 2 or larger than 4, the performance of ISML is not so satisfying. Similar trend can be found in pMCI versus NC classification as shown in Figs. 8(b) and 9(b), and also in pMCI versus sMCI classification as shown in Figs. 8(c) and 9(c). The underlying reason for those results could be that the inherent structure of an original class (e.g., AD, pMCI, sMCI, and NC) is not very complex; also, our experimental results are consistent with the results reported in [56] for AD/MCI classification. On the other hand, we can clearly see from Figs. 8 and 9 that the underlying data distribution may be not simple Gaussian distribution, as assumed by the conventional multitemplate-based methods, which justifies the proposed method.
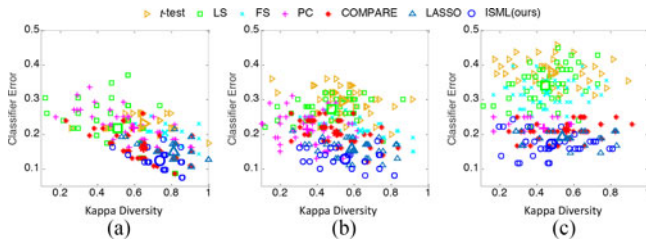
Fig. 10. Diversities and mean classification errors achieved by seven ensemble-based methods in (a) AD versus NC, (b) pMCI versus NC, and (c) pMCI versus sMCI classification tasks.

B. Analysis of Classifier Diversity

In this study, we propose an SVM-based ensemble classification method to better use multiview feature representation generated from multiple templates. To understand how the ensemble classification approach works, we now quantitatively measure the diversity and the mean classification error between any two different SVM classifiers, where each SVM is learned in a specific view space. Here, we use Kappa index to measure the diversity [59] of two classifiers, where a small Kappa value indicates a better diversity of two classifiers. Also, small mean classification errors imply better accuracies achieved by a pair of classifiers. In Fig. 10, we plot the Kappa-error diagrams and the corresponding centroids of point clouds achieved by seven ensemble-based methods in three classification tasks, where the most desired points lie on the bottom left of the Kappa-error diagram [59].

It can be seen from Fig. 10 that our ISML method consistently outperforms the compared methods in terms of the mean classification error in AD versus NC, pMCI versus NC, and pMCI versus sMCI classification tasks. Although LS, PC, and COMPARE usually achieve smaller Kappa values compared with ISML, their classification errors are much higher than those of ISML. These results indicate that the proposed ISML method makes a better tradeoff between the diversity and the classification error for achieving a better classification performance, compared with the other methods.

C. Limitations

In this study, we validate the efficacy of the proposed method via three groups of experiments and three binary classification tasks (i.e., the classifications of AD versus NC, pMCI versus NC, and pMCI versus sMCI). However, there are several limitations in our method.

First, using the proposed subclass clustering-based encoding method, we transform the original binary learning problem into a multitask learning problem. Here, we employ the OVA encoding strategy to relabel subjects, while there are still many other types of efficient encoding strategies for dealing with multiclass learning problems in machine learning domain (e.g., ternary encoding method and data-driven encoding strategy [60]). It is interesting to investigate whether other complex subclass encoding strategies can further boost the performance of AD/MCI classification.

Second, in the feature selection stage, we only use the naïve multitask sparse feature selection method with an $l_{2,1}$-norm-based regularizer, where relationships among subjects are not considered at all. As one type of prior information, the relationship information among subjects in each of multiple tasks can also be used to guide the feature selection procedure. For instance, it is possible to adopt the manifold regularized multitask feature selection model [47] to identify informative features, which is expected to further promote the performance of AD/MCI classification.

Third, we currently extract regional features in multiple template spaces, where the partitions of ROIs in different templates may be different from each other. The advantage of such feature extraction method is that the unique characteristics of different templates can be preserved naturally. However, at the same time, it is also difficult to directly compare subjects in two template spaces because of anatomical structure differences among templates. To facilitate direct comparison between subjects in two different template spaces, it could be interesting to further register those selected templates into a common space and then perform ROI partition jointly.

V. CONCLUSION

In this paper, we propose an ISML method with feature representation generated from multiple templates for AD/MCI classification. Specifically, we first select multiple templates from data and then extract multiview feature representation for subjects using those templates, where each template is treated as a specific view. Afterwards, we cluster subjects within each class into several subclasses in each view space and encode those subclasses with unique codes by considering both their original class information and their own distribution information, followed by a multitask feature selection procedure. Finally, we learn a view-specific SVM classifier using selected features in each view space and fuse results of multiple SVMs together by a majority voting strategy. We evaluate the efficacy of the proposed method on 459 subjects with MRI baseline data from the ADNI database and obtain the accuracies of 93.83%, 89.09%, and 80.90% for AD versus NC, pMCI versus NC, and pMCI versus sMCI classification tasks, respectively.

REFERENCES

[1] A. s. Association, "2013 Alzheimer's disease facts and figures," *Alzheimers Dementia*, vol. 9, pp. 208–245, 2013.

[2] N. Fox *et al.*, "Presymptomatic hippocampal atrophy in Alzheimer's disease A longitudinal MRI study," *Brain*, vol. 119, pp. 2001–2007, 1996.

[3] J. G. Sled *et al.*, "A nonparametric method for automatic correction of intensity nonuniformity in MRI data," *IEEE Trans. Med. Imag.*, vol. 17, no. 1, pp. 87–97, Feb. 1998.

[4] C. Gaser *et al.*, "Deformation-based morphometry and its relation to conventional volumetry of brain lateral ventricles in MRI," *NeuroImage*, vol. 13, pp. 1140–1145, 2001.

[5] B. C. Dickerson *et al.*, "MRI-derived entorhinal and hippocampal atrophy in incipient and very mild Alzheimer's disease," *Neurobiol. Aging*, vol. 22, pp. 747–754, 2001.

[6] A. D. Leow *et al.*, "Longitudinal stability of MRI for mapping brain change using tensor-based morphometry," *NeuroImage*, vol. 31, pp. 627–640, 2006.

[7] R. Cuingnet *et al.*, "Automatic classification of patients with Alzheimer's disease from structural MRI: A comparison of ten methods using the ADNI database," *NeuroImage*, vol. 56, pp. 766–781, 2011.

[8] R. Wolz *et al.*, "Multi-method analysis of MRI images in early diagnostics of Alzheimer's disease," *PloS One*, vol. 6, p. e25446, 2011.

[9] Y. Wang *et al.*, "Knowledge-guided robust MRI brain extraction for diverse large-scale neuroimaging studies on humans and non-human primates," *PloS One*, vol. 9, p. e77810, 2014.

[10] D. Zhang and D. Shen, "Multi-modal multi-task learning for joint prediction of multiple regression and classification variables in Alzheimer's disease," *NeuroImage*, vol. 59, pp. 895–907, 2012.

[11] J. Ashburner *et al.*, "Identifying global anatomical differences: Deformation-based morphometry," *Human Brain Mapping*, vol. 6, pp. 348–357, 1998.

[12] M. Chung *et al.*, "A unified statistical approach to deformation-based morphometry," *NeuroImage*, vol. 14, pp. 595–606, 2001.

[13] S. J. Teipel *et al.*, "Multivariate deformation-based analysis of brain atrophy to predict Alzheimer's disease in mild cognitive impairment," *NeuroImage*, vol. 38, pp. 13–24, 2007.

[14] J. Joseph *et al.*, "Three-dimensional surface deformation-based shape analysis of hippocampus and caudate nucleus in children with fetal alcohol spectrum disorders," *Human Brain Mapping*, vol. 35, pp. 659–672, 2014.

[15] C. Kipps *et al.*, "Progression of structural neuropathology in preclinical Huntington's disease: A tensor based morphometry study," *J. Neurol. Neurosurgery Psychiatry*, vol. 76, pp. 650–655, 2005.

[16] T. J. Whitford *et al.*, "Progressive grey matter atrophy over the first 2–3 years of illness in first-episode schizophrenia: A tensor-based morphometry study," *NeuroImage*, vol. 32, pp. 511–519, 2006.

[17] N. Leporé *et al.*, "Multi-atlas tensor-based morphometry and its application to a genetic study of 92 twins," in *Proc. Workshop Math. Foundations Comput. Anatomy*, New York, NY, USA, 2008, pp. 48–55.

[18] X. Hua *et al.*, "3D characterization of brain atrophy in Alzheimer's disease and mild cognitive impairment using tensor-based morphometry," *NeuroImage*, vol. 41, pp. 19–34, 2008.

[19] J. Koikkalainen *et al.*, "Multi-template tensor-based morphometry: Application to analysis of Alzheimer's disease," *NeuroImage*, vol. 56, pp. 1134–1144, 2011.

[20] X. Hua *et al.*, "Unbiased tensor-based morphometry: Improved robustness and sample size estimates for Alzheimer's disease clinical trials," *NeuroImage*, vol. 66, pp. 648–661, 2013.

[21] J. Ashburner and K. J. Friston, "Voxel-based morphometry—The methods," *NeuroImage*, vol. 11, pp. 805–821, 2000.

[22] C. Davatzikos *et al.*, "Voxel-based morphometry using the RAVENS maps: Methods and validation using simulated longitudinal atrophy," *NeuroImage*, vol. 14, pp. 1361–1369, 2001.

[23] G. Frisoni *et al.*, "Detection of grey matter loss in mild Alzheimer's disease with voxel based morphometry," *J. Neurol. Neurosurgery Psychiatry*, vol. 73, pp. 657–664, 2002.

[24] G. Chetelat *et al.*, "Mapping gray matter loss with voxel-based morphometry in mild cognitive impairment," *Neuroreport*, vol. 13, pp. 1939–1943, 2002.

[25] M. Bozzali *et al.*, "The contribution of voxel-based morphometry in staging patients with mild cognitive impairment," *Neurology*, vol. 67, pp. 453–460, 2006.

[26] A. Hämäläinen *et al.*, "Voxel-based morphometry to detect brain atrophy in progressive mild cognitive impairment," *NeuroImage*, vol. 37, pp. 1122–1131, 2007.

[27] J. C. Lau *et al.*, "Longitudinal neuroanatomical changes determined by deformation-based morphometry in a mouse model of Alzheimer's disease," *NeuroImage*, vol. 42, pp. 19–27, 2008.

[28] D. Shen and C. Davatzikos, "Very high-resolution morphometry using mass-preserving deformations and HAMMER elastic registration," *NeuroImage*, vol. 18, pp. 28–41, 2003.

[29] Y. Fan *et al.*, "COMPARE: Classification of morphological patterns using adaptive regional elements," *IEEE Trans. Med. Imag.*, vol. 26, no. 1, pp. 93–105, Jan. 2007.

[30] Y. Fan *et al.*, "Structural and functional biomarkers of prodromal Alzheimer's disease: A high-dimensional pattern classification study," *NeuroImage*, vol. 41, pp. 277–285, 2008.

[31] R. Min *et al.*, "Multi-atlas based representations for Alzheimer's disease diagnosis," *Human Brain Mapping*, vol. 35, pp. 5052–5070, 2014.

[32] M. Liu *et al.*, "View-centralized multi-atlas classification for Alzheimer's disease diagnosis," *Human Brain Mapping*, vol. 36, pp. 1847–1865, 2015.

[33] F. Lepore *et al.*, "Best individual template selection from deformation tensor minimization," in *Proc. IEEE Int. Symp. Biomed. Imaging, From Nano Macro*, 2008, pp. 460–463.

[34] R. Min *et al.*, "Maximum-margin based representation learning from multiple atlases for Alzheimer's disease classication," presented at the Med. Image Comput. Comput.-Assisted Intervention Conf., Boston, MA, USA, 2014.

[35] U. Noppeney *et al.*, "Identification of degenerate neuronal systems based on intersubject variability," *NeuroImage*, vol. 30, pp. 885–890, 2006.

[36] B. J. Frey and D. Dueck, "Clustering by passing messages between data points," *Science*, vol. 315, pp. 972–976, 2007.

[37] T. Kanungo *et al.*, "An efficient k-means clustering algorithm: Analysis and implementation," *IEEE Trans. Pattern Anal. Mach. Intell.*, vol. 24, no. 7, pp. 881–892, Jul. 2002.

[38] Y. Zhang *et al.*, "Segmentation of brain MR images through a hidden Markov random field model and the expectation-maximization algorithm," *IEEE Trans. Med. Imag.*, vol. 20, no. 1, pp. 45–57, Jan. 2001.

[39] M. Liu *et al.*, "Ensemble sparse classification of Alzheimer's disease," *NeuroImage*, vol. 60, pp. 1106–1116, 2012.

[40] D. Zhang *et al.*, "Multimodal classification of Alzheimer's disease and mild cognitive impairment," *NeuroImage*, vol. 55, pp. 856–867, 2011.

[41] D. Shen and C. Davatzikos, "HAMMER: Hierarchical attribute matching mechanism for elastic registration," *IEEE Trans. Med. Imag.*, vol. 21, no. 11, pp. 1421–1439, Nov. 2002.

[42] M. Liu *et al.*, "Hierarchical fusion of features and classifier decisions for Alzheimer's disease diagnosis," *Human Brain Mapping*, vol. 35, pp. 1305–1319, 2014.

[43] L. Shafarenko *et al.*, "Automatic watershed segmentation of randomly textured color images," *IEEE Trans. Image Process.*, vol. 6, no. 11, pp. 1530–1544, Nov. 1997.

[44] N. J. Nilsson, *Learning Machines*. New York, NY, USA: McGraw-Hill, 1965.

[45] F. Nie *et al.*, "Efficient and robust feature selection via joint l2,1-norms minimization," in *Proc. Conf. Adv. Neural Inf. Process. Syst.*, 2010, pp. 1813–1821.

[46] J. Liu *et al.*, *SLEP: Sparse Learning With Efficient Projections*. Tempe, AZ, USA: Arizona State Univ., 2009.

[47] B. Jie *et al.*, "Topological graph kernel on multiple thresholded functional connectivity networks for mild cognitive impairment classification," *Human Brain Mapping*, vol. 35, pp. 2876–2897, 2014.

[48] L. Lam and C. Y. Suen, "Application of majority voting to pattern recognition: An analysis of its behavior and performance," *IEEE Trans. Syst., Man Cybern. A, Syst. Humans*, vol. 27, no. 5, pp. 553–568, Sep. 1997.

[49] C. R. Jack *et al.*, "The Alzheimer's disease neuroimaging initiative (ADNI): MRI methods," *J. Magn. Reson. Imag.*, vol. 27, pp. 685–691, 2008.

[50] M. Jenkinson and S. Smith, "A global optimisation method for robust affine registration of brain images," *Med. Image Anal.*, vol. 5, pp. 143–156, 2001.

[51] M. Jenkinson *et al.*, "Improved optimization for the robust and accurate linear registration and motion correction of brain images," *NeuroImage*, vol. 17, pp. 825–841, 2002.

[52] I. Guyon *et al.*, "Gene selection for cancer classification using support vector machines," *Mach. Learn.*, vol. 46, pp. 389–422, 2002.

[53] X. He *et al.*, "Laplacian score for feature selection," in *Proc. Conf. Adv. Neural Inf. Process. Syst.*, 2005, pp. 507–514.

[54] C. M. Bishop, *Neural Networks Pattern Recognition*. Oxford, U.K.: Oxford Univ. Press, 1995.

[55] R. Tibshirani, "Regression shrinkage and selection via the Lasso," *J. Roy. Stat. Soc. B*, vol. 58, pp. 267–288, 1996.

[56] H.-I. Suk and D. Shen, "Subclass-based multi-task learning for Alzheimer's disease diagnosis," *Frontiers Aging Neurosci.*, vol. 6, pp. 1–12, Aug. 7, 2014.

[57] C.-C. Chang and C.-J. Lin, "LIBSVM: A library for support vector machines," *ACM Trans. Intel. Syst. Technol.*, vol. 2, p. 27, 2011.

[58] R. H. Fletcher *et al.*, *Clinical Epidemiology: The Essentials*. Baltimore, MD, USA: Williams & Wilkins, 2012.

[59] J. J. Rodriguez *et al.*, "Rotation forest: A new classifier ensemble method," *IEEE Trans. Pattern Anal. Mach. Intell.*, vol. 28, no. 10, pp. 1619–1630, Oct. 2006.

[60] O. Pujol *et al.*, "Discriminant ECOC: A heuristic method for application dependent design of error correcting output codes," *IEEE Trans. Pattern Anal. Mach. Intell.*, vol. 28, no. 6, pp. 1007–1012, Jun. 2006.

Authors' photographs and biographies not available at the time of publication.